J|A|C|S COMMUNICATIONS

Published on Web 03/12/2009

Optically Modulated Fluorophores for Selective Fluorescence Signal Recovery

Chris I. Richards, Jung-Cheng Hsiang, Dulal Senapati, Sandeep Patel, Junhua Yu, Tom Vosch, and Robert M. Dickson*

School of Chemistry and Biochemistry and Petit Institute for Biosciences and Bioengineering, Georgia Institute of Technology, Atlanta, Georgia 30332-0400

Received December 15, 2008; E-mail: dickson@chemistry.gatech.edu

Discriminating weak signals from large backgrounds confounds many fluorescence-based detection,[1−3] dynamics,[4,5] and structural applications.[6,7] Although fluorescence contrast is readily adaptable to both medical and biological imaging, sensitivity in deep tissue and intracellular imaging of low-copy-number proteins presents significant challenges. While great advances have been made,[4,5,8] available fluorophores too often access photostability- and emission-rate-impairing photoinduced dark states, thereby limiting interpretations.[9−11] However, controlled photoswitching to highly energy-recoverable, thermally stable, nonfluorescent isomers has been advantageously employed in the development of high-resolution optical serial localization methods,[6,7,12−14] and in stochastic switching-based optical lock-in detection (OLID) schemes.[15,16] Here we report dynamic photobrightening of fluorophores with photoaccessible but thermally *metastable* dark states that naturally decay on a 30 μs time frame. Under simultaneous near-IR (NIR) illumination, these metastable dark states are rapidly optically depopulated to directly and specifically modulate fluorescence at any externally applied frequency. Simultaneous demodulation of the entire epifluorescence image (i.e., digital signal processing-based lock-in detection for all pixels in parallel) specifically extracts weak-ensemble and even single-molecule fluorescence from high backgrounds.

Most photoswitching occurs through excited-state processes that stochastically trap a nonfluorescent isomer in a thermally stable configuration. Many applications of sequentially applied high-energy secondary excitation that stochastically recovers the original fluorescent state have been developed.[17,18] Unfortunately, the high-energy secondary beam required for switching simultaneously excites other emitters, generating significant additional background fluorescence unless applied when the sample is not being imaged. Additionally, switching is dependent on the laser intensity, forcing a compromise between bleaching and switching time to begin to approach biologically relevant time scales. Conversely, bulk fluorescence enhancement of organic dyes has been achieved via longer-wavelength but much less efficient optically induced reverse intersystem crossing.[19] Although potentially free of secondary-laser-induced additional background, such studies suffer from triplet reactivity, photoinstability, and exceedingly high, biologically incompatible secondary continuous-wave (cw) laser intensities (>1 MW/cm^2).[19] In contrast, single-stranded DNA (ssDNA)-encapsulated few-atom Ag nanodot-based fluorophores have all of the necessary components in place for such signal enhancements with vastly improved photostability and much lower incident intensities.[20−22] When encapsulated in ssDNA, nanoclusters or "nanodots" exhibit extremely bright fluorescence and excellent photophysics, yielding emission that is several-fold brighter and >10-fold more photostable than that obtainable from Cy3 or Cy5 while displaying only a single dark-state residence time of ~30 μs that itself shortens with increased primary excitation intensity.[22] In contrast to the use of alternating illumination with two high-energy wavelengths (relative to that of the detected fluorescence) and an internal standard to measure the demodulation waveform, as performed in OLID schemes, coillumination with an intensity-modulated, long-wavelength secondary laser dynamically photobrightens higher-energy nanodot emission. This secondary laser rapidly depopulates the dark state through transient absorption that regenerates the emissive manifold (see Figure 3S in the Supporting Information). This approach enables direct, noninterfering fluorescence modula-

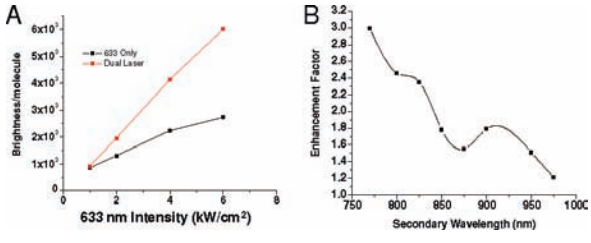

Figure 1. (A) Brightness per Ag nanodot under single-laser (633 nm, black) and dual-laser (633 nm + 805 nm, red) excitation, as determined by fluorescence correlation spectroscopy. Excitation becomes prematurely saturated as the 633 nm excitation intensity increases. Simultaneous 805 nm excitation (8 kW/cm^2) recovers the linearity between excitation and 710 nm emission. (B) Excitation scan of the secondary laser-based enhancement (4 kW/cm^2) relative to single-laser excitation (633 nm, 1.2 kW/cm^2).

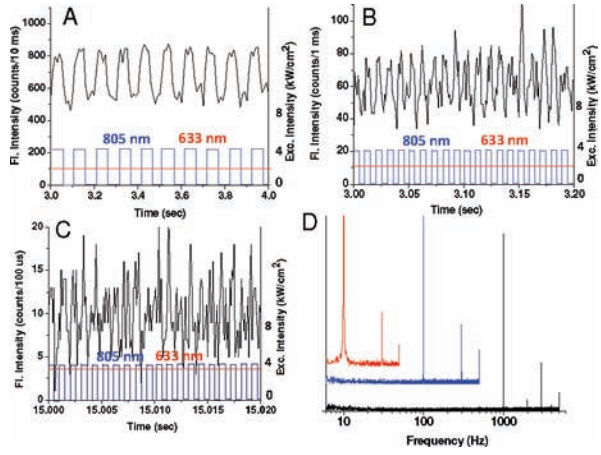

Figure 2. PVA-immobilized Ag nanodot emission collected with an APD in single-photon counting mode with constant 633 nm excitation and 805 nm excitation modulated at (A) 10, (B) 100, and (C) 1000 Hz. (D) Fourier transforms of the emission in (A−C) (red, blue, and green, respectively), each binned an order of magnitude faster than the modulation. The externally imposed 805 nm laser modulation results in the dynamic modulation of the fluorescence from the low-emission state to the high-emission state, with complete control down to short time regimes that is limited only by fluorophore brightness. With 1000 Hz modulation, the sample was cycled ~16 000 times with no decay in the fluorescence signal.

tion to uniquely and specifically detect bright Ag nanodot fluorescence buried within high backgrounds.

Aqueous solutions of few-atom Ag nanodots encapsulated in ssDNA with the sequence 5′-CCCTAACTCCCC-3′ [21] yielded spectrally pure, bright 710 nm emitters that were slightly blue-shifted in excitation but indistinguishable in size (~2.5 nm hydrodynamic radius, resulting mostly from the ssDNA scaffold) from those reported previously.[22,23] Intensity-dependent nanodot excitation at 633 nm revealed that not only on times but also off times (albeit at a reduced rate) decreased with increasing excitation intensity. Introduction of a non-background-producing secondary laser (805 nm) removed the dark-state-induced premature saturation (Figure 1A), producing up to 3-fold increases in fluorescence brightness per molecule relative to that with primary 633 nm

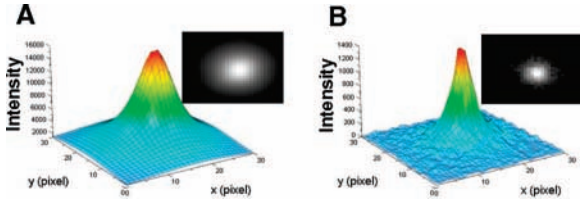

Figure 3. Ag nanodots imaged (60×, 1.2 NA, Andor iXon EMCCD, 16 μm pixels) through a highly concentrated Cy5 solution with constant defocused 633 nm excitation (3 kW/cm^2) and optically chopped and focused 805 nm excitation (2 kW/cm^2). (A) 3D plot of a typical raw 10 ms exposure ccd frame. Inset: raw 2D ccd image. (B) 3D plot of the demodulated signal with a time constant of 1 s, exclusively recovering the much weaker Ag nanodot signal (2% of the total signal at the brightest pixel). Inset: 2D image of same 10 ms frame. The secondary laser was chopped at 10 Hz, and images were synchronized to the modulation and collected at 100 Hz for 10 s. The recovered image is roughly the same size (5 pixels fwhm) as the 805 nm laser spot size, demonstrating the background elimination and demodulated nanodot signal recovery.

excitation alone. Fluorescence enhancement with such low-energy, low-intensity secondary excitation has not been reported with other fluorophores.

For a detailed analysis of the fluorescence enhancement, nanodots were dispersed in poly(vinyl alcohol) (PVA) and excited at 633 nm (1.2 kW/cm^2). Simultaneous excitation with tunable cw secondary laser yielded a significant enhancement of the ~710 nm emission across the entire excitation range, with an excitation maximum near 775 nm (Figure 1B). This excitation spectrum also appears quite similar to the absorption spectrum of anionic cytosine,[24,25]which is also readily optically depopulated with long-wavelength excitation. In order to minimize the overlap with the fluorescence collected at higher energy while yielding significant enhancement, 805 nm secondary excitation with laser-line filtering was utilized in the majority of the experiments. While typical samples composed of a few molecules in the laser focus under 1.6 kW/cm^2, 633 nm excitation easily yielded ~60 000 detected photons/s (Figure 2A−C), simultaneously optically chopped (at 10, 100, or 1000 Hz, corresponding to Figure 2A−C, respectively) 805 nm illumination dynamically modulated the emission rate perfectly in phase with the secondary laser modulation. The lower emissive intensity corresponded to that for the 633 nm excitation alone, and the higher levels occurred only with dual-laser illumination (Figure 2A−C). Fourier transforms of the resulting time traces revealed the original laser modulation frequency in each case (Figure 2D). This dynamic photobrighting is in stark contrast to OLID[15,16] and other static photoswitching methods,[6,7,16−18] as the emission is dynamically cycled between bright and brighter states, precisely at and in phase with the externally applied modulation frequency, without an increase in background. The brighter level is achieved as long as the fluorophores are coilluminated with the non-background-generating secondary laser. In contrast, photoswitches exhibit stochastic on and off times and need alternating illumination with primary and secondary light, both of which have higher energy than the collected fluorescence, thereby precluding external dynamic control of modulation cycles.[15,16] Demodulation of the nanodot emission is readily performed at any imposed modulation frequency to uniquely and specifically recover the nanodot fluorescence from the (unmodulated) background with greatly reduced noise.

Although direct nanodot excitation at 633 nm gives strong emission, the non-background-generating modulation of 700−800 nm Ag nanodot emission enables extremely weak signals to be extracted from a much brighter background. As the emission of Cy5 is essentially indistinguishable from that of our Ag nanodots, we imaged nanodot emission localized in a thin PVA film through a highly concentrated solution of Cy5. When only 633 nm excitation was focused on the nanodot/PVA sample, >60 000 counts per pixel were observed on the ccd camera, primarily from out-of-focus Cy5 emission (Figure 3A). Introduction of the same-diameter 805 nm laser also focused on the PVA film increased the intensity on the brightest pixel by only a few percent, yet chopping of the 805 nm laser coupled with 10-fold faster synchronous wide-field imaging and simultaneous demodulation of every pixel signal in parallel (whole image demodulation) allowed observation only of the signal from the much lower concentration Ag nanodots with very high contrast (Figure 3B). The recovered image was roughly the same size (5 pixels fwhm) as the 633 and 805 nm laser spot sizes on the PVA film, demonstrating excellent rejection of unmodulated Cy5 emission. The demodulated image resulted only from that area of the Ag nanocluster PVA film that was coilluminated with the 805 nm laser.

The same synthetic procedure also yields photophysically indistinguishable Ag nanodots in 5′-biotinylated oligomers of the same sequence. Low-density cell-surface biotinylation followed by fixation and labeling with avidin enabled cell surfaces to be sparsely

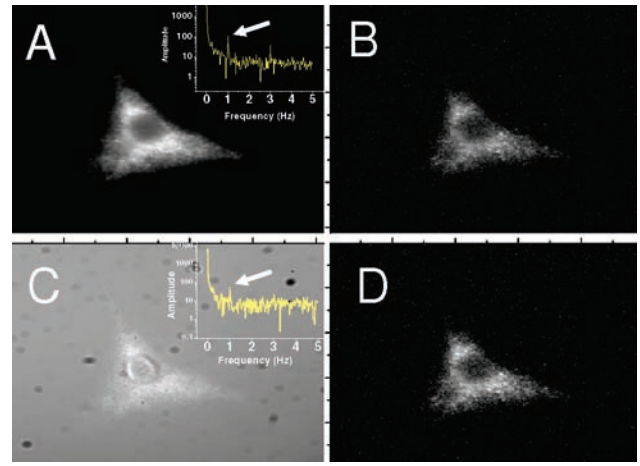

Figure 4. (A) Typical dual-laser ccd image of biotinylated NIH 3T3 cells surface-labeled with avidin and biotinylated Ag nanodots. The secondary laser modulates the fluorescence at every pixel simultaneously. Inset: Fourier transform of a typical pixel intensity as a function of time. (B) Autofluorescence is removed from the recovered cell image after demodulation at the modulation frequency [indicated by the arrow in the inset of (A)] using only three modulation cycles. (C) Image of the same cell with highly concentrated Cy5 solution added to simulate a very high autofluorescent background. Inset: the modulation frequency remains readily apparent in the Fourier transform of a typical pixel intensity vs time. (D) Demodulated image (30 modulation cycles) showing the nearly complete elimination of the Cy5 and autofluorescent background signals, leaving only the distinct signal of the Ag nanodots.

labeled with Ag nanodots emitting at 710 nm. Highly localized, small, and sometimes blinking signals suggestive of individual molecules were readily observed on top of significant autofluorescence (Figure 4A). Wide-field epifluorescent imaging and modulation were performed with overlapped, defocused primary- and secondary-laser excitation. Secondary excitation (805 nm) was chopped at 1 Hz, and emission (710 nm) was imaged with

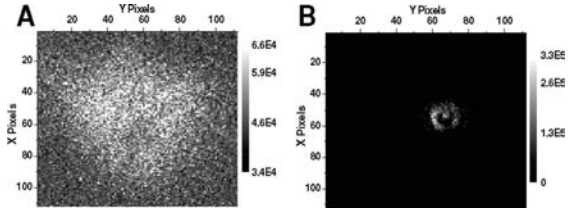

Figure 5. (A) Cy 5 (200 nM) and Ag nanodots emitting at 710 nm (~500 pM) in a PVA film imaged [1.4 NA, 150× total magnification, Andor iXon (front illuminated), 7.8 mM pixels, 40 Hz] under constant 633 nm excitation (800 W/cm^2) and simultaneous 805 nm excitation (6 kW/cm^2) optically chopped at 4 Hz. (A) Representative 25 ms frame of the combined signal from separate imaging of Cy5 (200 nM solution) and an individual Ag nanodot (defocused to show a characteristic single-molecule dipole emission pattern), both in PVA. Excitation and imaging were performed identically for each, with constant 633 nm excitation (2 kW/cm^2) and 805 nm excitation (6 kW/cm^2) chopped at 4 Hz along with synchronous 40 Hz ccd detection. (B) Demodulated image (10 s time constant) clearly showing the otherwise unobservable single-nanodot dipole emission pattern without the large background.

synchronous 10-fold faster ccd detection. The modulation frequency was readily apparent in the Fourier transform of the intensity trajectory of any given pixel (Figure 4A, inset), clearly showing that modulation enables detection away from the lower-frequency noise present in fluorescence imaging. Demodulation at the chopping frequency directly yielded images with greatly improved signal-to-noise ratios, as (unmodulated) autofluorescent background was removed after as few as three modulation cycles (Figure 4B). In order to create a higher-background environment, Cy5 solution was added to the same sample and imaged in an identical manner. Imaging through the bright Cy5 solution obscured the single-nanodot signals (Figure 4C), but the modulation frequency was still readily apparent in the Fourier transform (Figure 4C, inset). Even in the presence of bright inhomogeneous background fluorescence, demodulation again recovered the nanodot images (Figure 4D), suggesting single-nanodot sensitivity on fixed cell surfaces.

Although we readily observed single-molecule-suggestive signals after whole-image demodulation of nanodot fluorescence (e.g., Figure 4S in the Supporting Information), verification of single nanodot sensitivity in such high-background samples is challenging. Therefore, separate samples of single nanodots (~500 pM) diluted and spun in PVA and of 200 nM Cy5 similarly diluted and spun in PVA were prepared and separately imaged under identical modulation and detection conditions. Films containing only Ag nanodots at this concentration yielded well-resolved individual molecules exhibiting clear dipole emission patterns when slightly defocused,[26,27] indicating single-molecule observation. Separately imaged Cy5 samples yielded only a bright homogeneous background. The Cy5 background and Ag nanodot dipole emission data sets were added, and the resulting ccd images (Figure 5A) showed that the dipole emission patterns were completely obscured by the background. Subsequent demodulation readily recovered the original dipole emission patterns, indicating true single-molecule signal extraction from a high background (Figure 5B) and great promise for intracellular single-molecule imaging.

These unique biocompatible nanomaterials not only enable extremely high sustainable count rates through optically induced depopulation of a photoaccessed dark state but also possess fast response times that enable long-wavelength, high-frequency modulation of dark-state residence, thereby dynamically increasing the fluorescence intensity. Such NIR modulation of these red−NIR emitters provides a unique digital-signal-processing-based method of extracting weak signals from extremely high background images, opening a significant number of single-molecule and potentially bulk medical-imaging applications.

Acknowledgment. R.M.D. gratefully acknowledges financial support from NIH R01-GM086195. C.I.R. acknowledges NIH NRSA F31EB008324 support, and T.V. acknowledges an FWO fellowship.

Note Added after ASAP Publication. This paper was published ASAP March 12, 2009, before a final correction was incorporated. The current version shows the full revision.

Supporting Information Available: Experimental methods, autocorrelations of single molecules with one- and two-laser excitation, and pixel intensity as a function of time with resulting Fourier transforms for single-molecule and ensemble demodulation. This material is available free of charge via the Internet at http://pubs.acs.org.

References

(1) Taik Lim, Y.; Kim, S.; Nakayama, A.; Stott, N. E.; Bawendi, M. G.; Frangioni, J. V. *Mol. Imaging* **2003**, *2*, 50–64.
(2) Tokunaga, M.; Imamoto, N.; Sakata-Sogawa, K. *Nat. Methods* **2008**, *5*, 455–455.
(3) Sako, Y.; Minoghchi, S.; Yanagida, T. *Nat. Cell Biol.* **2000**, *2*, 168–172.
(4) Kural, C.; Kim, H.; Syed, S.; Goshima, G.; Gelfand, V. I.; Selvin, P. R. *Science* **2005**, *308*, 1469–1472.
(5) Elf, J.; Li, G. W.; Xie, X. S. *Science* **2007**, *316*, 1191–1194.
(6) Bates, M.; Huang, B.; Dempsey, G. T.; Zhuang, X. *Science* **2007**, *317*, 1749–1753.
(7) Betzig, E.; Patterson, G. H.; Sougrat, R.; Lindwasser, O. W.; Olenych, S.; Bonifacino, J. S.; Davidson, M. W.; Lippincott-Schwartz, J.; Hess, H. F. *Science* **2006**, *313*, 1642–1645.
(8) Myong, S.; Bruno, M. M.; Pyle, A. M.; Ha, T. *Science* **2007**, *317*, 513–516.
(9) Hoogenboom, J. P.; van Dijk, E.; Hernando, J.; van Hulst, N. F.; Garcia-Parajo, M. F. *Phys. Rev. Lett.* **2005**, *95*, 097401.
(10) Schmidt, T.; Kubitscheck, U.; Rohler, D.; Nienhaus, U. *Single Mol.* **2002**, *3*, 327.
(11) Bates, M.; Blosser, T. R.; Zhuang, X. W. *Phys. Rev. Lett.* **2005**, *94*, 108101.
(12) Hu, D.; Tian, Z.; Wu, W.; Wan, W.; Li, A. D. Q. *J. Am. Chem. Soc.* **2008**, *130*, 15279–15281.
(13) Steinhauer, C.; Forthmann, C.; Vogelsang, J.; Tinnefeld, P. *J. Am. Chem. Soc.* **2008**, *130*, 16840–16841.
(14) Dedecker, P.; Hotta, J.-i.; Flors, C.; Sliwa, M.; Uji-i, H.; Roeffaers, M. B. J.; Ando, R.; Mizuno, H.; Miyawaki, A.; Hofkens, J. *J. Am. Chem. Soc.* **2007**, *129*, 16132–16141.
(15) Mao, S.; Benninger, R. K. P.; Yan, Y. L.; Petchprayoon, C.; Jackson, D.; Easley, C. J.; Piston, D. W.; Marriott, G. *Biophys. J.* **2008**, *94*, 4515–4524.
(16) Marriott, G.; Mao, S.; Sakata, T.; Ran, J.; Jackson, D. K.; Petchprayoon, C.; Gomez, T. J.; Warp, E.; Tulyathan, O.; Aaron, H. L.; Isacoff, E. Y.; Yan, Y. *Proc. Natl. Acad. Sci. U.S.A.* **2008**, *105*, 17789–17794.
(17) Hess, S. T.; Girirajan, T. P. K.; Mason, M. D. *Biophys. J.* **2006**, *91*, 4258–4272.
(18) Biteen, J. S.; Thompson, M. A.; Tselentis, N. K.; Bowman, G. R.; Shapiro, L.; Moerner, W. E. *Nat. Methods* **2008**, *5*, 947–949.
(19) Ringemann, C.; Schonle, A.; Giske, A.; von Middendorff, C.; Hell, S. W.; Eggeling, C. *ChemPhysChem* **2008**, *9*, 612–624.
(20) Yu, J.; Choi, S.; Dickson, R. M. *Angew. Chem., Int. Ed.* **2009**, *48*, 318–320.
(21) Richards, C. I.; Choi, S.; Hsiang, J. C.; Antoku, Y.; Vosch, T.; Bongiorno, A.; Tzeng, Y. L.; Dickson, R. M. *J. Am. Chem. Soc.* **2008**, *130*, 5038–5039.
(22) Vosch, T.; Antoku, Y.; Hsiang, J. C.; Richards, C. I.; Gonzalez, J. I.; Dickson, R. M. *Proc. Natl. Acad. Sci. U.S.A.* **2007**, *104*, 12616–12621.
(23) Petty, J. T.; Zheng, J.; Dickson, R. M. *J. Am. Chem. Soc.* **2004**, *126*, 5207–5212.
(24) Raytchev, M.; Mayer, E.; Amann, N.; Wagenknecht, H. A.; Fiebig, T. *ChemPhysChem* **2004**, *5*, 706–712.
(25) Schiedt, J.; Weinkauf, R.; Neumark, D. M.; Schlag, E. W. *Chem. Phys.* **1998**, *239*, 511–524.
(26) Bartko, A. P.; Dickson, R. M. *J. Phys. Chem. B* **1999**, *103*, 11237–11241.
(27) Hassey, R.; Swain, E. J.; Hammer, N. I.; Venkataraman, D.; Barnes, M. D. *Science* **2006**, *314*, 1437–1439.

JA809785S